Supporting Information

Continuous fabrication of MOF-based memory elements via droplet microfluidic synthesis

Alina Kuleshova[a,+], Irina Koriakina[a,+], Anastasia Lubimova[a], Maria Timofeeva[a], Ekaterina Gunina[a], Kirill Bogdanov[b], Ivan Reznik[a], Svyatoslav A. Povarov[a], Soslan Khubezhov[a], Dmitriy Guzei[c], Andrey Minakov[c], Kazumi Toda-Peters[d], Amy Q. Shen[d], Valentin Milichko[a,e]*, and Mikhail V. Zyuzin[a,]*

[a]School of Physics and Engineering, ITMO University, St. Petersburg, Russia

[b]International Research and Education Center for Physics of Nanostructures, ITMO University, Saint Petersburg 197101, Russia

[c]Siberian Federal University, Krasnoyarsk, Russia

[d]Micro/Bio/Nanofluidics Unit, Okinawa Institute of Science and Technology Graduate University, Onna, Japan

[e]Université de Lorraine, Centre National de la Recherche Scientifique (CNRS), F-54000 Nancy, France

[+]equal contribution

*corresponding authors: mikhail.zyuzin@metalab.ifmo.ru, v.milichko@metalab.ifmo.ru

Table S1. MOF-based memristors.[1,2]

Structure	Method of fabrication	V_{set} (V)	MOF thickness (μm)	ON/OFF ratio	Ref.
ITO/AuNP@Cd-MOF/Ag	spin-coating	2.1 - 4.8	1.5	10^2 - 10^4	[3]
Si/Zif-8/Ag	dip coating	2.45	0.06	10^7	[4]
Au/Zif-8/Al	dip coating	1.9	0.2	10^4	[5]
Au/Zif-8/Ag	dip coating	1.8	0.3	10^8	[6]
FTO/PVA@2-MIM-Zif-8@PEG/Ag	dip coating	1.3	0.3	80	[7]
Pt/RSMOF-1/W	solvothermal	7.5	10 - 25	30	[8]
Ag/FJU-23-H2O/Ag	solvothermal	0.2	45	10^5	[9]
ITO/Zif-8@PVPy/Ag	solution	1.24	0.2	$7.8*10^3$	[10]
Ag/Rb-CD-MOF/Ag	vapor deposition	2	1000	150	[11]
FTO/UiO-66@PVA/Ag	microwave	0.37	0.5	10^4	[12]

1. Materials and Methods

a. Materials

Reagents for MOF synthesis were purchased from Merck: $Cu(NO_3)_2$×2.5 H_2O (≥98.0%), benzene-1,3,5-tricarboxylic acid or trimesic acid (95%, H_3BTC), N,N-Dimethylformamide (99.8%, DMF), and ethanol (≥99.5%, EtOH, ACS reagent). We also used fluorinated oil Fluoridrop 40 (Dolomite Microfluidics, UK), emulsion stabilizers (008-FluoroSurfactant, RAN Biotechnologies), and chloroform (Lenreaktiv, Russia).

b. Preparation of precursors for the microfluidic synthesis

For microfluidic synthesis, 77.6 mg $Cu(NO_3)_2$ and 2 ml of DMF were added into a 2 ml microcentrifuge tube and put into an ultrasonic bath until fully dissolved. Then, 119 mg H_3BTC and 5 ml DMF were added into the tube and put into an ultrasonic bath until fully dissolved.

c. Reference microwave synthesis of HKUST-1

H_3BTC (105,1 mg, 0.50 mmol) was dissolved in 25 mL DMF and 25 mL EtOH to form 10 mM of *Solution A*. Then, $Cu(NO_3)_2 \times 2.5\ H_2O$ (174 mg, 0.75 mmol) was dissolved in 25 mL DMF and 25 mL EtOH to form 15 mM of *Solution B*. Afterwards, 2.5 mL of *Solution A* and 2.5 mL of *Solution B* were mixed in a 10 mL test tube. The test tubes were put in a microwave synthesizer (Discover SP,CEM Corporation) for 10 min at 90 W and 60°C. After 10 min, the reaction mixture was transferred to a 15 mL centrifuge tube, isolated by the centrifugation (10 000 rpm for 5 min), and washed with 10 mL of DMF and EtOH three times. The solid sample was dried at 60°C for 24 h.

2. Microfluidic chip (MFC) fabrication

The glass microfluidic devices were fabricated using a subtractive 3D printing process known as selective laser-induced etching (SLE).[13,14] This two-step fabrication process involves volumetric femto-second pulsed laser irradiation within a solid glass substrate followed by chemical etching to remove unwanted material. The microfluidic device design was created using Rhinoceros 3D modeling software (Robert McNeel & Associates Inc.), scanned within the volume of a polished 5 mm thick fused silica substrate (Optostar Japan) using the commercially available LightFab 3D printer (LightFab GmbH). The patterned fused silica substrate was then ultrasonicated in 8 mol/l potassium hydroxide at 85 °C for 135 h.[13]

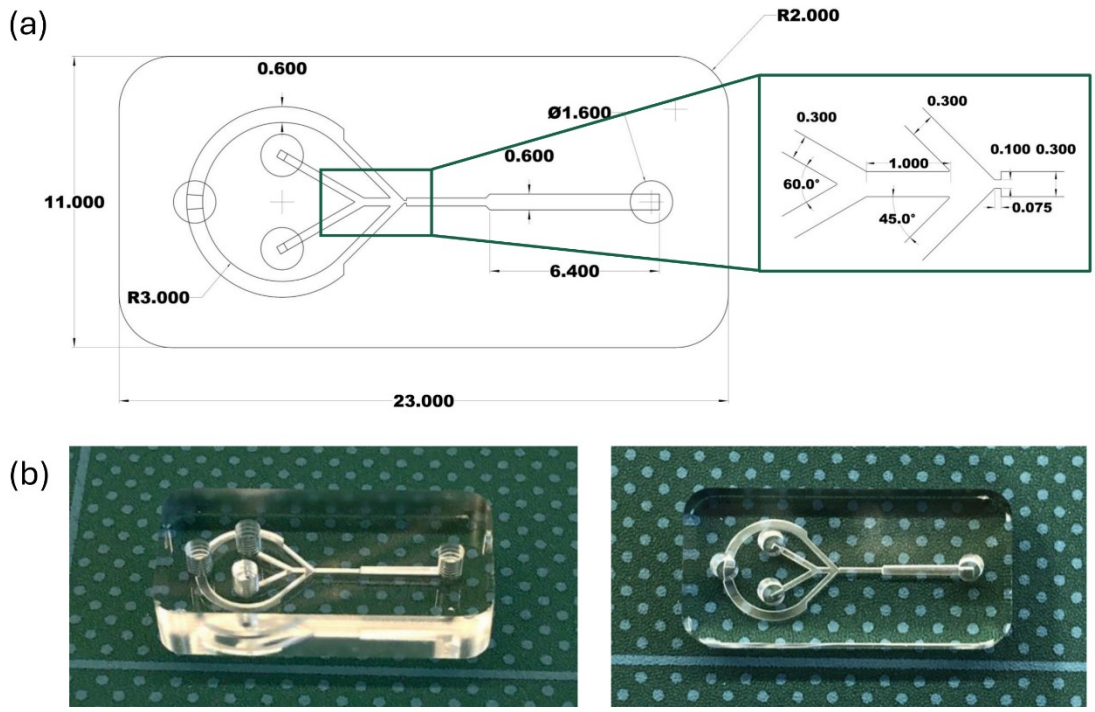

Figure S1. Image of a glass MFC fabricated via selective laser etching technology. (a) Geometry of the MFC, (b) digital images of an MFC.

3. Surfactant selection

The surfactant concentration was determined experimentally using a model system. Emulsion stabilizer 008-Fluorosurfactant was added to fluorinated oil Fluoridrop 40 (continuous phase) at concentrations of 3 wt%, 6 wt%, and 12 wt%. Meanwhile, DMF was used as the dispersed phase. By adjusting the flow rate ratios of the reagents (Q_c and Q_d), the regimes for forming uniform droplets were defined (**Figure S2**).

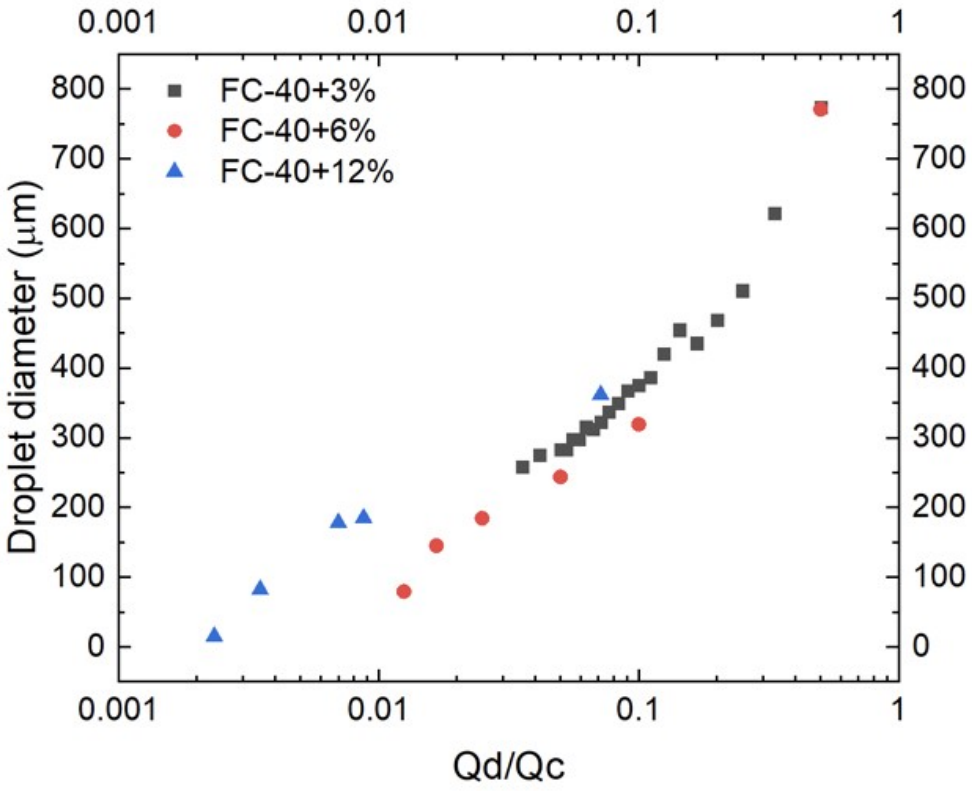

Figure S2. Experimental selection of the optimal concentration of surfactant.

4. Numerical simulation of droplets formation

A numerical study of the flow regimes of dimethylformamide (DMF) and fluorinated oil Fluoridrop 40 in a microchannel was carried out using Ansys software. Calculations were carried out in a laminar flow regime in a three-dimensional setting. To simulate two-phase flow in a microchannel, the Volume of fluid (VOF) method was used.[15] This approach allows modeling an immiscible multicomponent liquid-liquid flow, solving the problem of momentum conservation and using the volume fraction of each phase. The volume fraction of dimethylformamide C_{DMF} and the volume fraction of Fluidrop 40 C_F obey the condition $C_{DMF}+C_F=1$.

During the calculation process, a system of equations is solved.

Mass conservation equation:

$$\frac{\partial(\rho\vec{V})}{\partial t} + \nabla(\rho\vec{V}) = 0, \quad (1)$$

where $\vec{V}$ is the mixture velocity vector; to determine it, an equation of momentum is solved:

$$\frac{\partial(\rho\vec{V})}{\partial t} + \nabla(\vec{V}\vec{V}) = -\nabla p + \nabla[\mu(\nabla\vec{V} + \nabla\vec{V}^{T})] + \vec{F_{ca}}, \quad (2)$$

where *p* is the static pressure of the mixture and $\vec{F_{ca}}$ is the vector of the volumetric force caused by capillary forces.

The transport equation is solved to simulate the movement of the interface between the phases of the DMF–Fluidrop 40 flow:

$$\frac{\partial C_F}{\partial t} + (C_F\vec{V}) = 0, \quad (3)$$

To describe the flow of immiscible liquids, taking into account the capillary forces is crucial. To model surface tension, the continuous surface force (CSF), we used the algorithm of Brackbill et al.[16] The effects of surface tension were modeled by adding a source to the momentum equation:

$$\vec{F_{ca}} = \sigma\kappa\nabla C_F, \quad (4)$$

where σ is the coefficient of interfacial tension and κ is the curvature of the interface.

On the walls of the computational domain, the normal vector is determined using the following expression:

$$\vec{n} = \vec{n_W}cos(\theta) + \vec{\tau_W}sin(\theta), \quad (5)$$

where θ is the wetting angle of the wall, $\vec{n_W}$ is the vector perpendicular to the wall, and $\vec{\tau_W}$ is the vector tangentially directed to the wall.

The calculations used the experimentally determined dependence of interfacial tension on the temperature of the DMF–Fluoridrop 40 system. These measurements were carried out using an IFT-820-P automatic tensiometer. The dependences of the viscosity and density of dimethylformamide on temperature were specified using the Dortmund Data Bank.[17] For Fluoridrop 40, the dependence of physical properties on temperature was specified according to the manufacturer's data.[18]

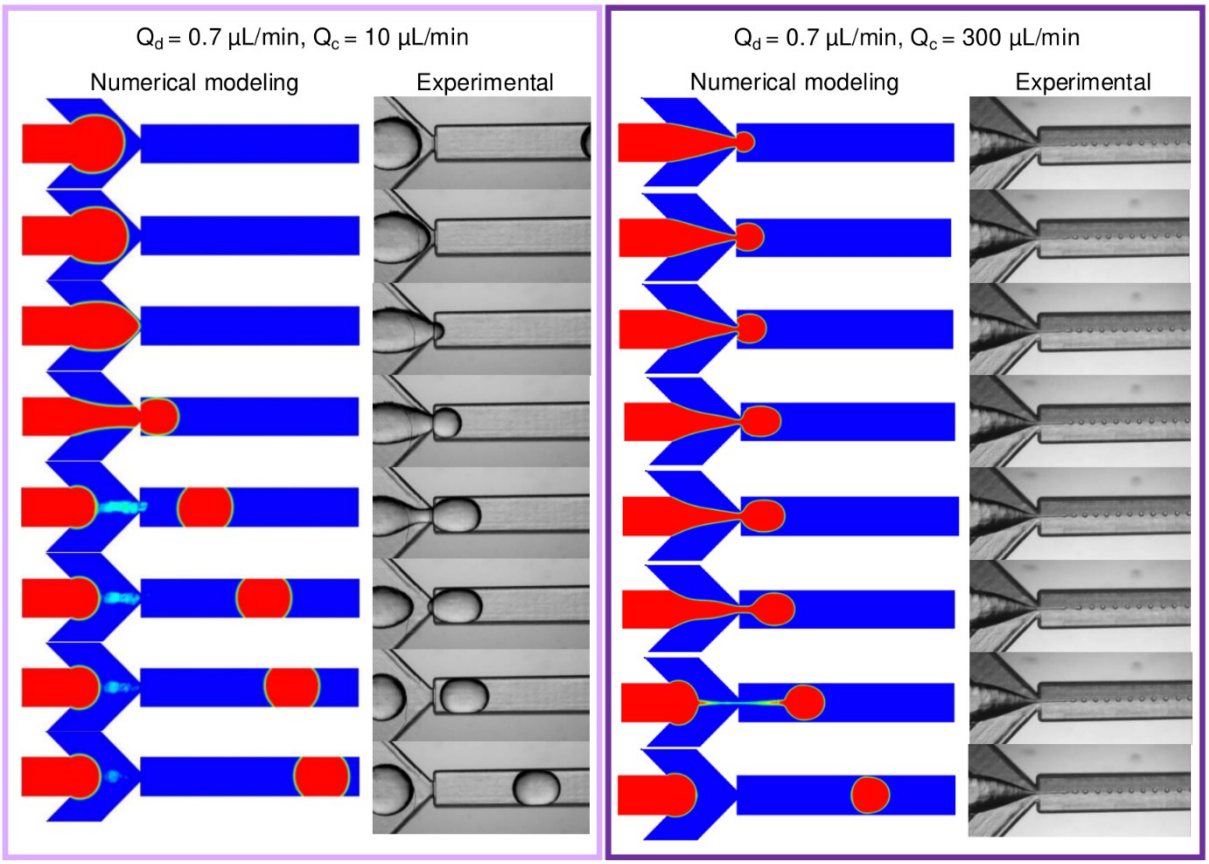

Figure S3. Comparison of numerical modeling of droplet formation with experimental data on droplet generation at different flow rates of reagents and different time points during and after droplet formation.

To describe the process of transfer and mixing of copper nitrate $Cu(NO_3)_2$ and H_3BTC by DMF, the transfer equations for the concentration of this component were additionally introduced into the system of equations (only within DMF):

$$\frac{d(\rho Y_i)}{dt} + \nabla \cdot (\rho \vec{V} Y_i) = \nabla(D\rho\nabla Y_i), \quad (6)$$

where Y_i is the concentration of the i-component and D is the diffusion coefficient.

This allowed us to take into account the processes of transfer and mixing of $Cu(NO_3)_2$ and H_3BTC dissolved in DMF.

As boundary conditions at the inputs to the micromixer, a speed value corresponding to the experimental conditions was set. For the entrances to the microchannel where DMF was supplied, in addition to the velocity value, the corresponding concentration values of copper

(II) nitrate and trimesic acid were specified. At the exit from the computational domain, Neumann conditions were specified. On the channel walls, the adhesion condition was set.

To solve the system of nonlinear differential equations (1-3), the FVM method (Finite Volume Method) was used. The relationship between the velocity field and pressure is implemented using the SIMPLEC algorithm. To calculate the continuity balance, we used the PRESTO! (PREssure STaggering Option) scheme. An implicit second-order scheme was used to approximate the nonstationary terms of the transport equations. To approximate the convective terms of the Navier-Stokes equations, a second-order central-difference scheme was used. To solve the transport equation, a second-order scheme was used. A structured computational grid consisting of 1,000,000 nodes was used. The time step size was determined based on the conditions CFL < 1 (Courant–Friedrichs–Lewy).

5. Microfluidic synthesis setup

For the synthesis of HKUST-1 MOFs via droplet microfluidics method, the reagents were supplied into a glass MFC through PTFE capillary system and controlled using syringe pumps (Pump 11 Elite, Harvard Apparatus, USA). The dispersed phase (MOF precursors: $Cu(NO_3)_2$ and H_3BTC dissolved in DMF) was introduced into inlet 1 and 2 of the MFC, while the continuous phase (fluorinated oil) was introduced into inlet 3. Droplet formation was observed using an optical microscope with a high-speed camera (Phantom Miro C110, Vision Research, USA). The synthesized MOF microcrystals were collected into a collection tube containing 2 ml of chloroform.

To wash the synthesized MOF microcrystals from fluorinated oil, a chloroform solution with HKUST-1 MOFs residing in it was removed from the initial tube with the residual fluorinated oil. After that, the solution was centrifuged at 10 000 rpm for 3 min using Microspin 12 (BioSan, Latvia), the supernatant was removed, and 2 ml of chloroform were added. Then the solution was sonicated and centrifuged again. These steps were repeated twice. Finally, the obtained microcrystals were dispersed in 300 µl of DMF.

a. Temperature variation

The scheme of the setup used for synthesis at different temperatures is shown in **Figure S4**. Heating of the droplet generation region was carried out using a microheater that is heated when connected to a power source. The microheater was fabricated by screen printing

technology, in which carbon inks and silver paste were applied onto dense paper. Prior to use, the microheater was calibrated using a thermocouple.

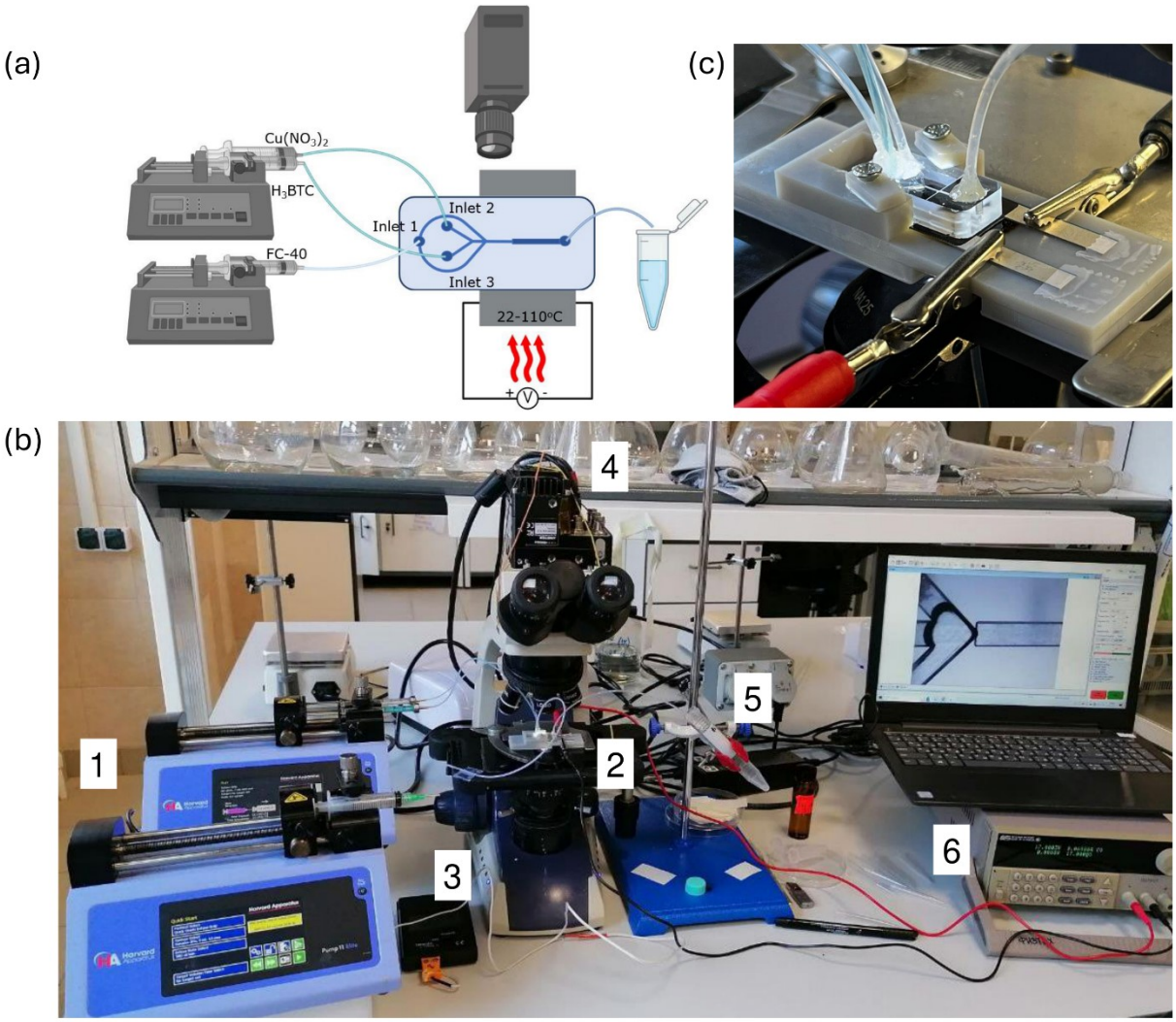

Figure S4. Synthesis setup. (a) Schematic representation of the synthesis setup; (b) photo of the synthesis setup with (1) syringe pumps, (2.1) glass MFC, (2.2) microheater, (3) optical microscope, (4) high-speed camera, (5) product collection tube, and (6) power source; (c) MFC assembled with a microheater.

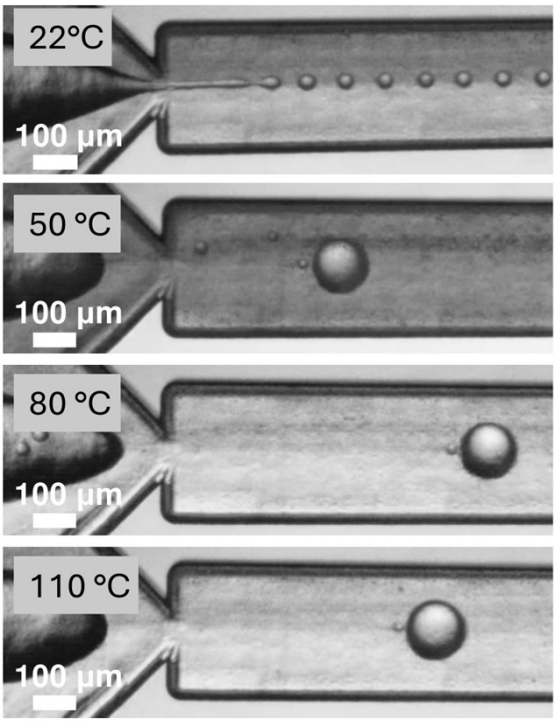

Figure S5. Variation of droplet diameters with increasing applied temperature.

b. Flow rates variation

The scheme of the experimental setup used for synthesis at different flow rates in channels is shown in **Figure S6**.

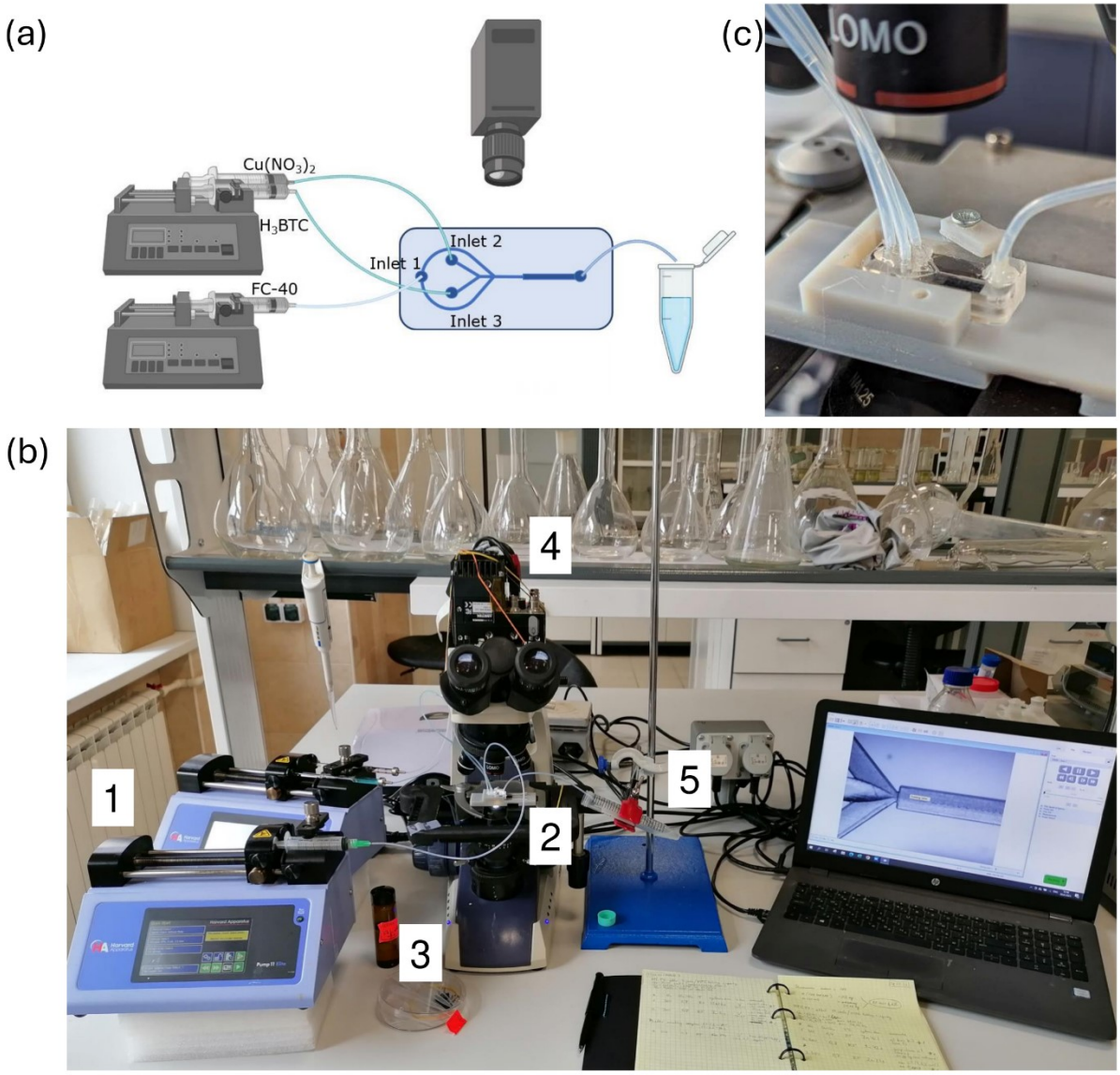

Figure S6. Synthesis setup. (a) Schematic representation of the synthesis setup; (b) photo of the synthesis setup with (1) syringe pumps, (2) glass MFC, (3) optical microscope, (4) high-speed camera, and (5) product collection tube; (c) glass MFC.

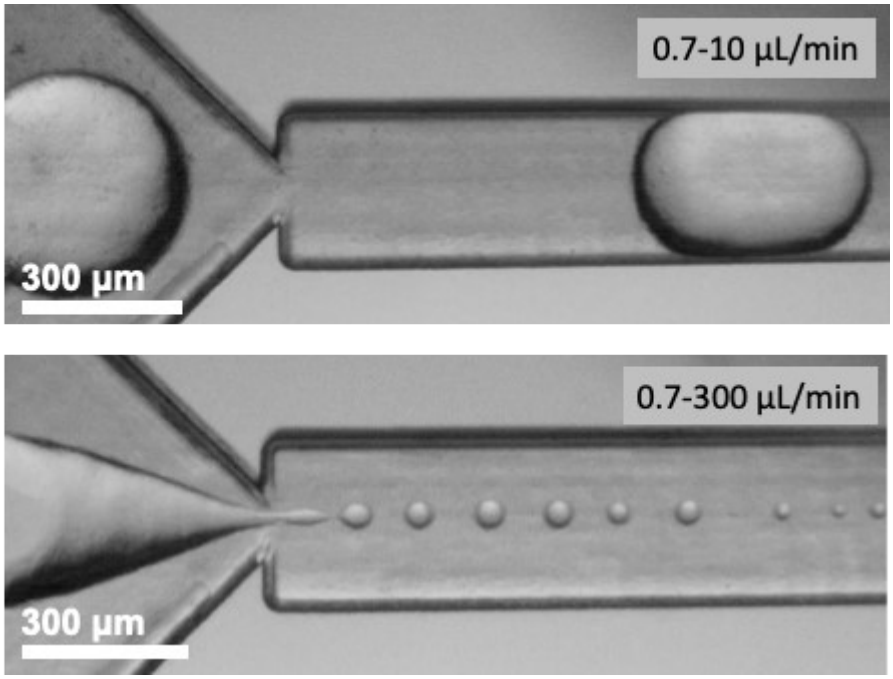

Figure S7. Variation of droplet diameters with increasing flow rate ratio.

c. Capillary length variation

An experiment was conducted to investigate the influence of time on the synthesis of MOFs. To vary the reaction time, we used capillaries of two different lengths: (i) 20 mm and (ii) 200 mm. Given the inner diameter of the capillary tubes was 1 mm and the carrier fluid flowed at a constant rate of 300 µL/min, we estimated droplet residence times of 10 seconds and 100 seconds for the 20 mm and 200 mm length capillary tubes, respectively. After synthesis, the resulting MOFs were analyzed using SEM (**Figure S8**).

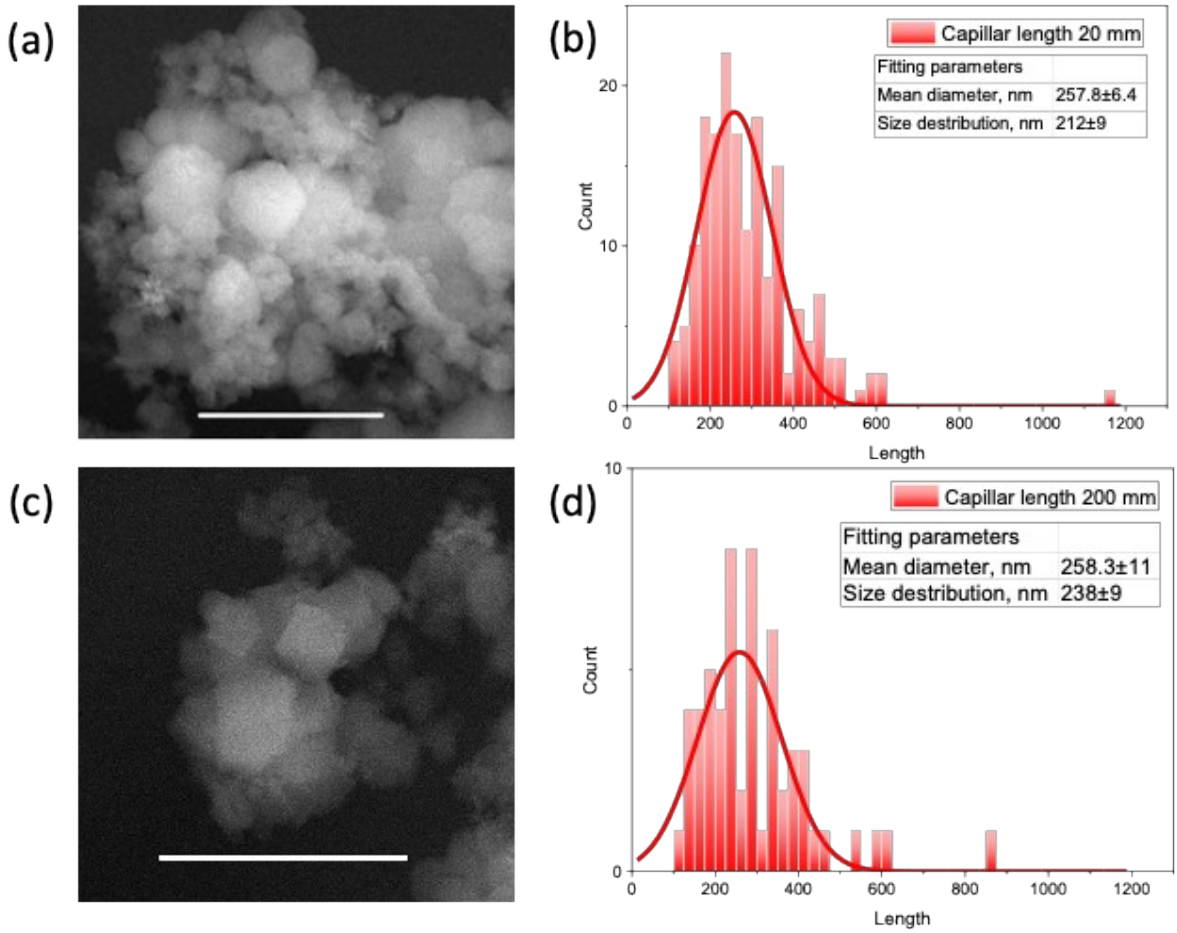

Figure S8. SEM images (a, c) and size distributions (b, d) of HKUST-1 nanoparticles synthesized at different reaction time (10 (a, b) and 100 (c, d) seconds). Bar length is set to 200 nm.

SEM images analysis showed a similar mean size of 257±6 nm and 258±11 between synthesis with 10- and 100-s residence time, respectively. Simultaneously we register a slight increase in size distribution. To determine, whether the differences in MOFs sizes from both syntheses were significant, we performed Students' t-test analysis using null-hypothesis of identity in mean size between two syntheses with different residence time:

$$t = \frac{\overline{x_1} - \overline{x_2} - \Delta}{\sqrt{\frac{s_1^2}{n_1} + \frac{s_2^2}{n_2}}} \quad (7)$$

where x_1 and x_2 are the means of the two samples, Δ is the hypothesized difference between the population means (0 in our case of testing for equal means), s_1 and s_2 are the standard

deviations of the two samples and n_1 and n_2 are the sizes of the two samples. **Table S2** contains all parameters used for calculation t-score.

Table S2. Parameters of the Students' t-test analysis.

Residence time, s	N	X	S
10	57	294	135
100	176	294	125
t-score	0.04		
Degree of freedom	231		
Probability	96.47%		

In case of comparison size distributions of HKUST-1 synthesis with 10 and 100 s residence time we achieved t-value of 0.04 and with degree of freedom equal to 231 we have the possibility of null-hypothesis of 96.47 %. With that we can conclude that changes in droplets' residence time in capillary tubes has only an insignificant effect on mean size synthesized nanoparticles.

6. Scanning electron microscopy (SEM)

For SEM analysis, HKUST-1 microcrystals were deposited onto Si substrates and dried. SEM measurements were carried out using MERLIN (Carl Zeiss, Germany) with an acceleration voltage of 2 kV. The obtained SEM images were analyzed to estimate the average linear size of microcrystals with the ImageJ software.

Additionally, MOFs obtained by the microwave synthesis approach were imaged with a SEM (Quanta 200, FEI, Netherlands) with an acceleration voltage of 25 kV. For this, MOFs were also previously deposited onto Si substrates and covered with an Au layer.

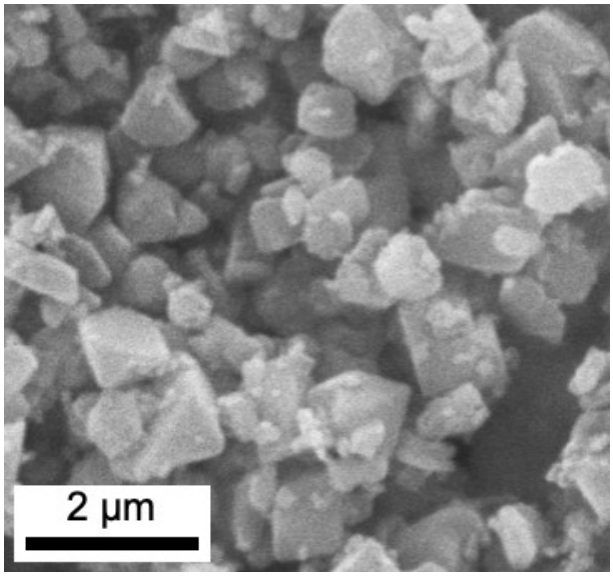

Figure S9. SEM of MOFs obtained by microwave synthesis method.

7. Powder X-ray diffraction (pXRD) analysis

For the analysis of the crystalline structure, MOFs were deposited onto cover glass substrates. To carry out pXRD, an Ultima IV X-ray diffractometer (Rigaku, Japan) was used. The radiation wavelength of the copper anode is CuK_{α} = 1.5418 Å. Measurements were performed in the range of 5-30 degrees with a step of measurement 0.01 degrees, and the measurement speed was 0.1 degrees/min. The Crystallography Open Database was used to identify the phase.
For the samples obtained via microfluidic approach, the dimensions of the crystalline phase were determined using the Scherrer formula:

$$d = \frac{K\lambda}{\beta cos\theta} \qquad (8)$$

D is the crystallite size;
K is the Scherrer constant, K=0.94;
λ is the wavelength of X-ray radiation;
β is the width of the reflex at half maximum;
Θ is the diffraction angle.

Table S3. Crystallite size of HKUST-1 for each synthesis temperature.

T, °C	D, nm
22	72.53 ± 25.15
50	80.12 ± 24.15
80	67.70 ± 15.53
110	71.45 ± 17.62

The magnitude of the relative microstrain of the lattice was calculated using the formula:

$$\frac{\Delta d}{d} = \frac{\beta}{4tan\theta} \qquad (9)$$

Table S4. Datasets for microstrain evaluation based on pXRD.

T, °C	Peak position, 2Θ (°)	FWHM, β (°)	Microstrain, $\Delta d/d \cdot 10^3$
22	6.73	0.17	12.9
	9.52	0.16	8.6
	11.70	0.07	3.3
	13.49	0.16	6.0
	17.57	0.09	2.6
50	6.73	0.14	10.5
	9.53	0.14	7.5
	11.71	0.07	3.2
	13.50	0.12	4.8
	17.58	0.08	2.4
80	6.72	0.15	11.5

	9.52	0.14	7.4
	11.68	0.09	4.2
	13.48	0.13	5.1
	17.55	0.10	2.9
110	6.74	0.13	10.1
	9.52	0.15	8.0
	11.69	0.08	3.6
	13.49	0.13	5.0
	17.56	0.09	2.7

Additionally, diffraction patterns of MOFs obtained via microwave synthesis method were recorded using a Bruker D2 Phaser X-ray diffractometer with a 300 W characteristic CuK_{α} ($K_{\alpha 1}$ λ = 1.54184 Å, angular range 2θ = 5°-30°) X-ray radiation source and a BraggBrentano goniometer geometry. The angular resolution during the analysis was 0.3 degree at a scanning speed of 1 degrees/min (**Figure S10**).

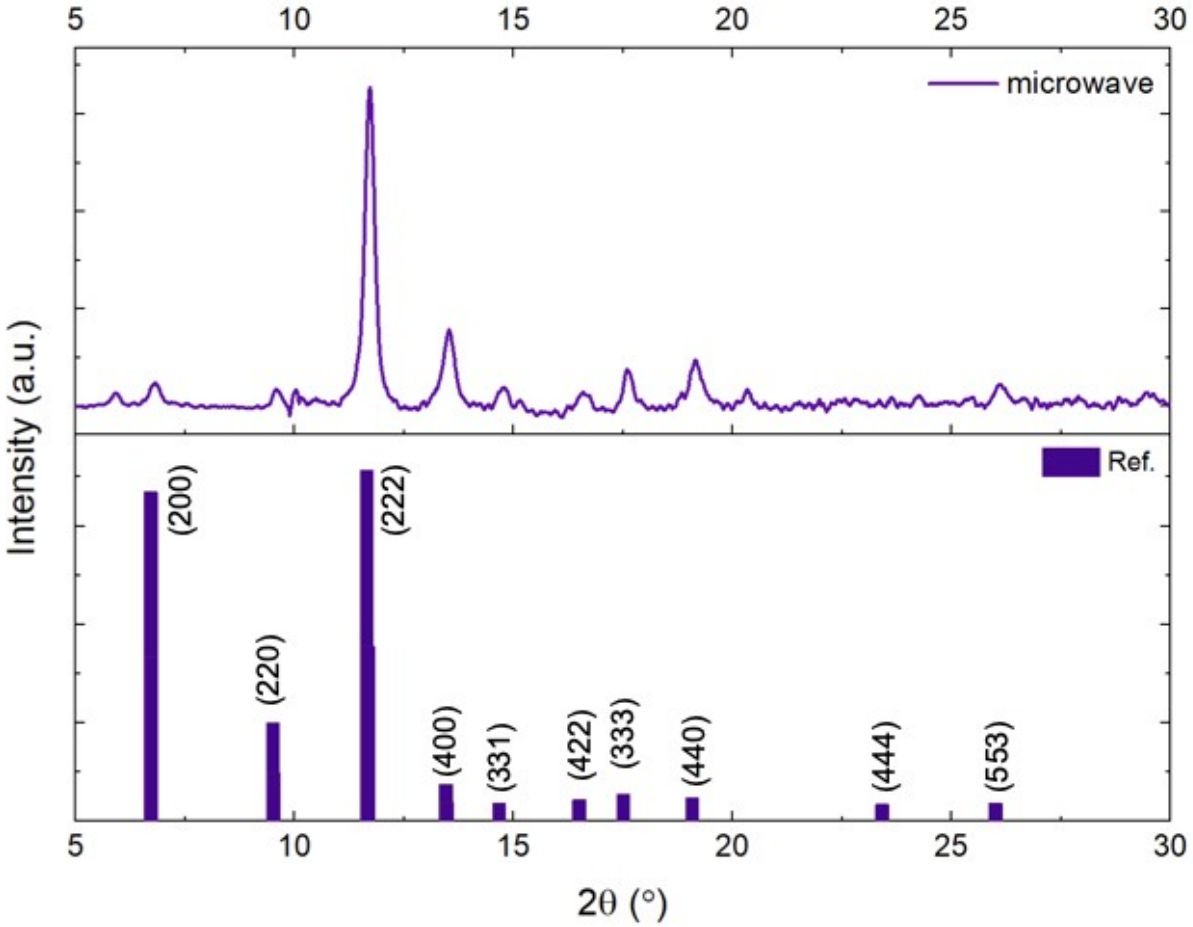

Figure S10. pXRD of MOFs HKUST-1 crystals obtained by **microwave** synthesis approach [19], (CCDC 943008).

8. Dynamic light scattering (DLS)

The hydrodynamic diameter of MOFs synthesized using the microwave method was estimated using the DLS approach. For this purpose, MOFs were dispersed in 1 ml of deionized water at concentration 1 mg/ml, and the hydrodynamic diameter (D_h, nm) was measured using a Photocor Complex (Russia) equipped with a semiconductor laser operating at 638 nm (P=25 mW). Each measurement was performed at 25°C during 90 s.

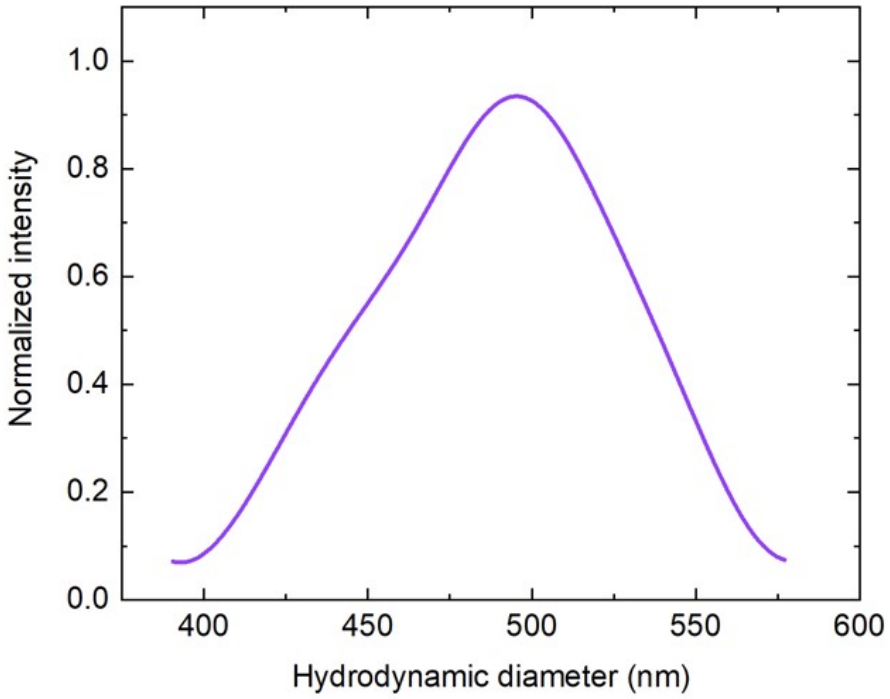

Figure S11. DLS hydrodynamic size distribution of MOFs obtained by microwave synthesis approach.

The hydrodynamic diameter of MOFs synthesized using the microfluidic method also was estimated using the DLS approach. DLS measurements were conducted on Photocor Complex (Photocor, Russia). Before analysis samples were dissolved in DMF and sonicated for 5 min and placed in a 4 mL vial. In order to achieve stable measurements data accumulation for correlation function was set to 5 min. All measurements were conducted in 160 degree beam setup (back scattering) and at 22 °C. After measurements, correlation function was fitted with double extrapolation method, in order to extract distribution of hydrodynamic radius of HKUST-1 nanocrystals. Fitting range was set from 30 to 200 channels.

Table S5. Summarized hydrodynamic distribution analysis of HKUST-1 nanocrystals obtained at different temperatures.

	Area, nm	**Mean, nm**	**Position, nm**	**STD**
22 °C	0.525	550.4	564.7	118.5
50 °C	0.058	372.6	349.2	79.40
80 °C	0.369	383.8	348.4	57.51
110 °C	0.078	295.5	295.0	56.07

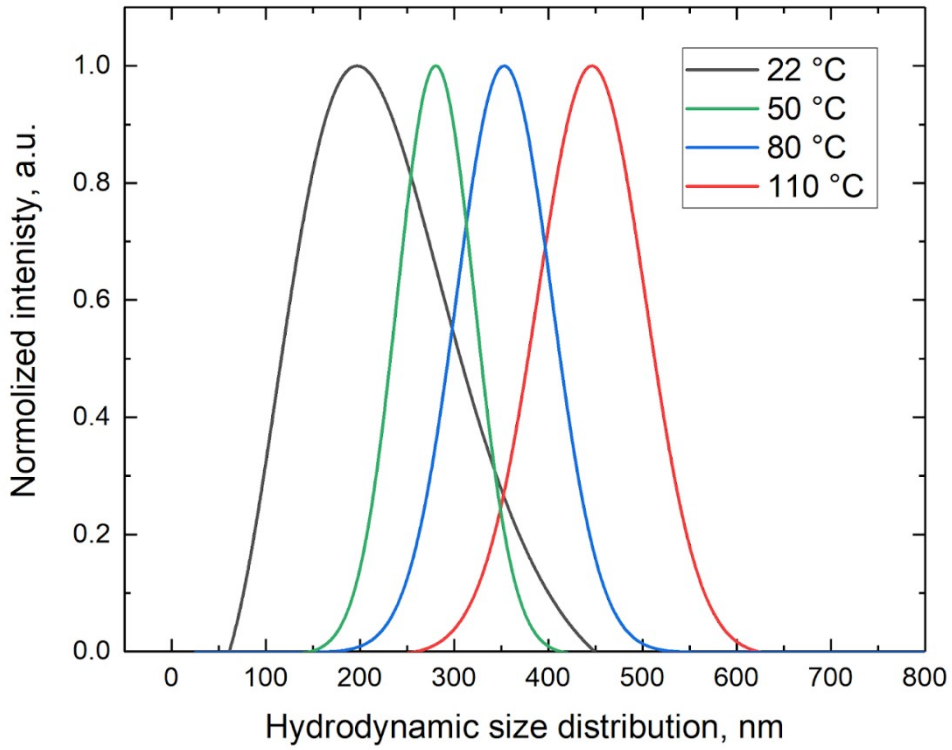

Figure S12. Hydrodynamic HKUST-1 size distribution dependence from synthesis temperature.

9. X-ray photoelectron spectroscopy (XPS) measurements

XPS measurements of the MOFs microcrystals were carried out on an Escalab 250Xi photoelectron spectrometer equipped with an AlKα monochromatic radiation source (photon energy 1486.6 eV). The spectrometer was calibrated against the Au 4 f7/2 line (binding energy 84.0 eV). The spectra were recorded in the constant transmission energy mode at 50 eV with an XPS spot size of 650 μm. The total energy resolution of the experiment was about 0.3 eV. The studies were carried out at room temperature in an ultrahigh vacuum of the order of 1-10^{-9} mbar. To remove the sample charge, a combined ion-electronic charge compensation system was used.

Table S6. The surface composition of the samples obtained from high-resolution spectra.

Sample	F1s	C1s	O1s	Cu2p3	Si2p	N1s
22°C	40.7	39.1	17.3	1.8	0.6	0.5

50°C	15.7	50.6	26.7	5.7	0.8	0.5
80°C	22.0	47.7	24.3	5.0	0.5	0.5
110°C	9.2	51.9	29.0	6.8	2.6	0.5
Microwave	0.46	54.73	32.68	7.9	3.31	0.91

Table S7. Calculated components ratio of C1s high resolution XPS, in %.

C-C	C=O	C-O
60.7	35.4	3.9
60.24	35.88	3.88
60.6	35.5	3.9
59.6	36.4	4.0
59.48	36.9	3.62

10. ReRAM analysis

For the ReRAM analysis, the HKUST-1 microcrystals obtained with either microfluidic or microwave methods were deposited onto gold (Au) substrates acting as electrodes. Initially, a 5 nm layer of chromium (Cr) was sputtered onto cleaned glass for improved adhesion, followed by a 100 nm layer of Au. Then, a 3 μm wide groove was made by the laser ablation method. The depth of the groove provides complete isolation between the Au electrodes. Then, HKUST-1 microcrystals were placed in the gap by drop casting method.

To examine the memristive properties of the crystals, a ReRAM Tester setup that enabled automated data measurement was used (RR Robotics, Russia). This setup involved the use of a modified programming power supply (0-45 V, compliance 0.1 A) equipped with an integrated voltmeter and ammeter to provide a constant voltage. Additionally, the setup featured a controller for automating measurements, enabling control over the power source voltage and polarity. Data acquisition was performed using a Keithley 2700 multimeter with a sensitivity of 10 nA. Data collection was conducted with a 0.5 V step and a 1-second interval for both synthesis methods.

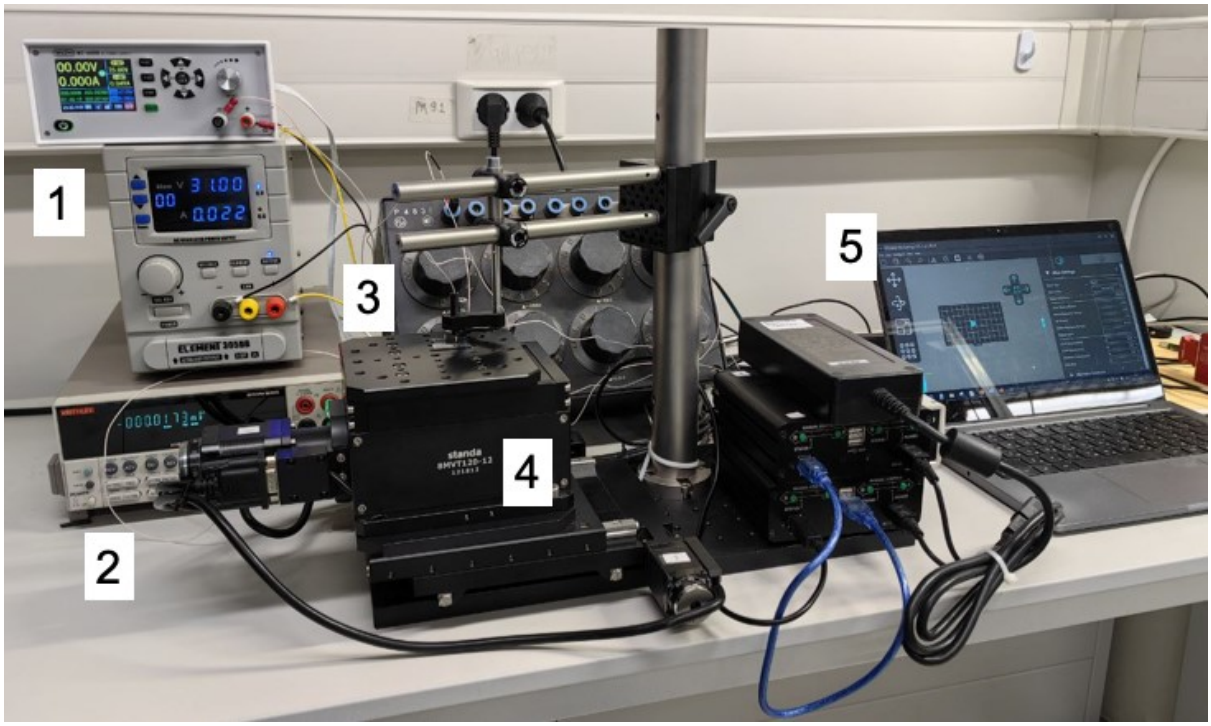

Figure S13. ReRAM Tester setup. (1) Power supply with built-in controllers (CPU), (2) multimeter, (3) shunt resistor (R_s), (4) movable table for sample positioning, (5) all the data are collected using the designed software.

To ensure accurate measurements, test cells were isolated to prevent displacement of microcrystals within the groove (**Figure S14**).

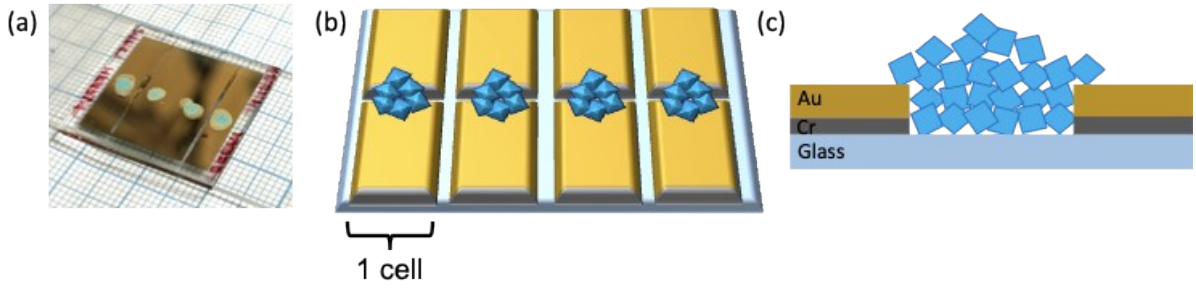

Figure S14. Memristive element used to measure ReRAM. (a) Photograph of the memristive elements with deposited HKUST-1 crystals, (b) schematic view of the memristive elements showing MOFs located on the substrate divided into several cells, (c) schematic view of a memristive element showing MOFs located in the groove created by laser ablation.

Additionally, time stability of the memristive elements (microfluidic HKUST-1 on Au substrate) were measured. This parameter is primarily determined by the crystals' ability to incorporate water into their pores, but other factors like UV light may also play a role. We performed the following experiment to address the question:

(i) Two control groups of crystals on Au substrates were selected. One sample was placed in an inert nitrogen atmosphere to exclude water aggregation into the MOF pores, while the second group was exposed to a humid environment. Weekly measurements of the current-voltage characteristics were performed. **Figure S15** presents I-V curves for one of the samples stored in the humid environment after 1 week and after 2 weeks. During this period, the memristor retained its electronic properties (ON/OFF ratio even increased slightly in 2 weeks), albeit with decreasing switching voltage, Vset, (from 21.5-23 V to 7-10 V).

(ii) Herein, **figure S16** demonstrates I-V curves for a sample stored in a dry box. This sample displayed minimal change in its memristive properties. This stability suggests that ReRAM cells based on microfluidic HKUST-1 are promising candidates for applications in low-humidity environments. This experimental observation was also confirmed by Raman spectroscopy (**Figure S20**), which reveals a characteristic peak associated with the presence of water in the pores of samples stored in humid conditions[22].

(iii) We also realized an accelerated aging experiment: microfluidic HKUST-1 crystals were soaked in water for one hour, three days after the final stability experiment (**Figure S17**). Subsequent measurements of I-V curves demonstrated that the samples did not lose their memristive properties.

After two weeks, the retention time was measured for both groups (**Figure S18**). The sample stored in the dry box exhibited a retention time for the low resistance state (LRS) that was twice high compared with the sample stored in a wet environment. For this experiment, the switching voltage (V_{set}) to the low resistance state was chosen to be 40 V, and the reading voltage (V_{read}) was set to 3 V (3 s after switching to V_{set}). Notably, HKUST-1, stored in a wet environment, switched to LRS slower (>7 μs) than the dry sample (<1 μs).

Finally, averaging across all samples from both groups, we plotted the dependence of the average ON/OFF ratio for memristive switching as a function of time from the start of the experiment (**Figure S19**). The sample stored in an inert atmosphere potentially retains its memristive properties for a long time compared to the crystals stored in a wet atmosphere.

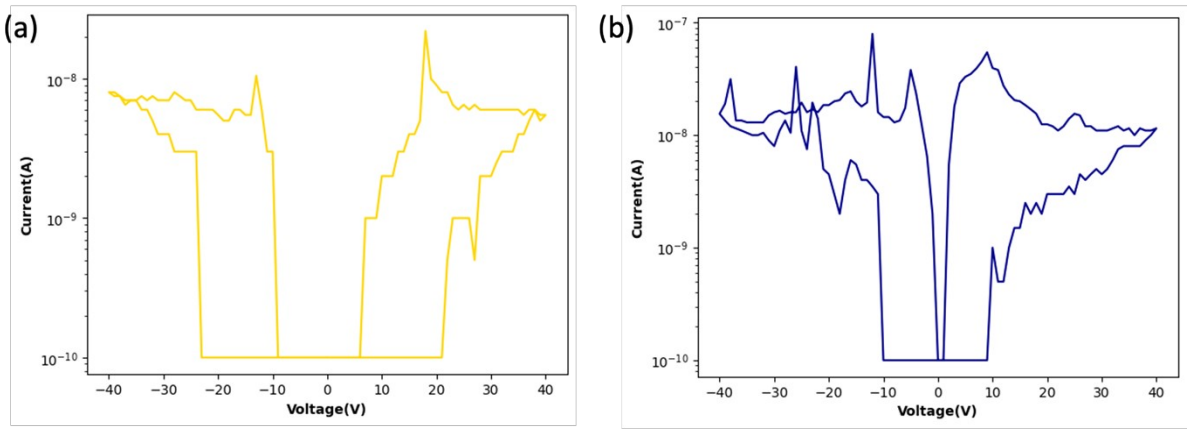

Figure S15. I-V curves for the memristor (microfluidic HKUST-1 on a Au substrate) exposed to a humid environment: (a) after 1 week and (b) after 2 weeks.

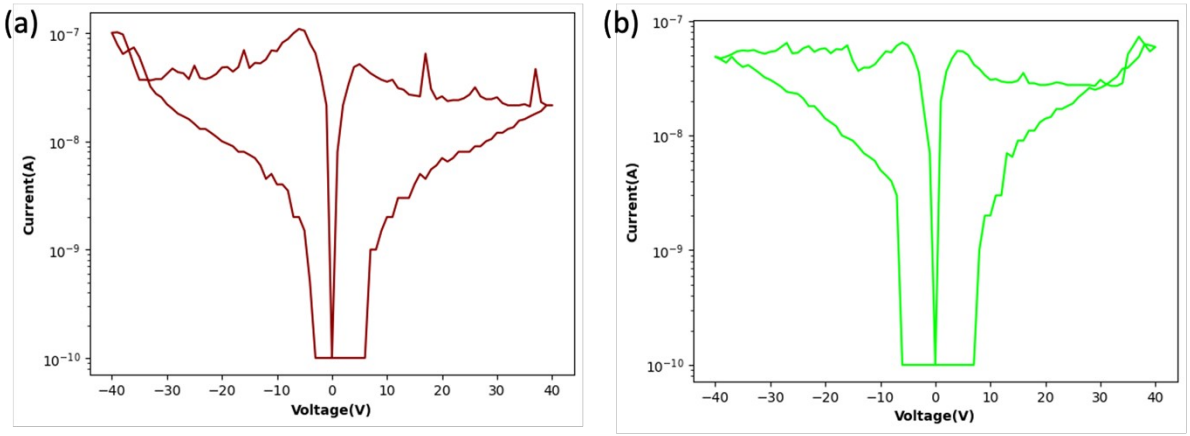

Figure S16. I-V curves for the memristor (microfluidic HKUST-1 on a Au substrate) placed in an inert nitrogen atmosphere: (a) after 1 week and (b) after 2 weeks.

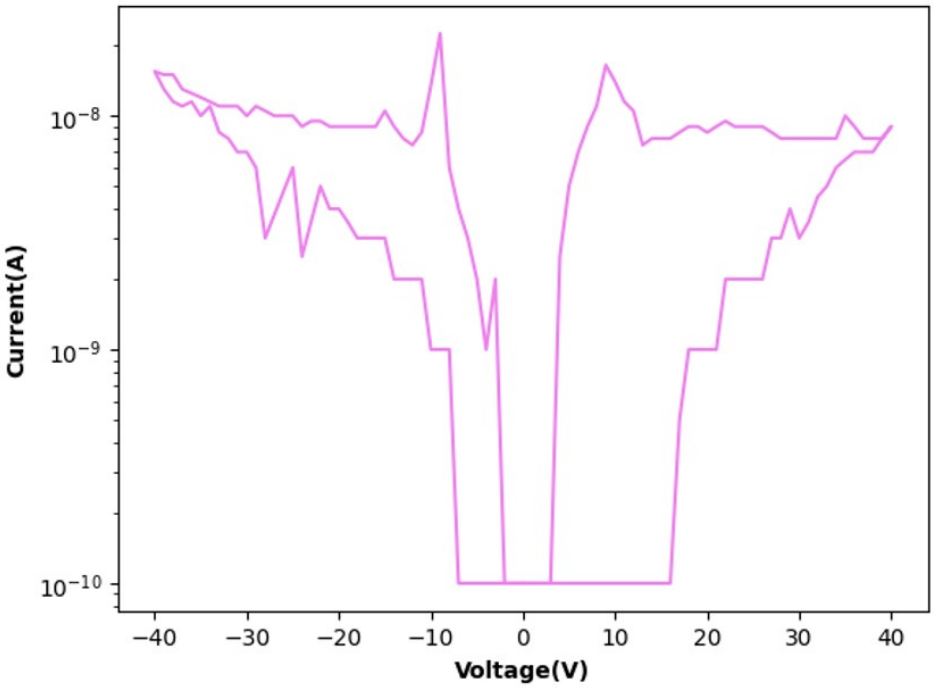

Figure S17. I-V curves for the memristor (microfluidic HKUST-1 on a Au substrate) after an accelerated aging experiment.

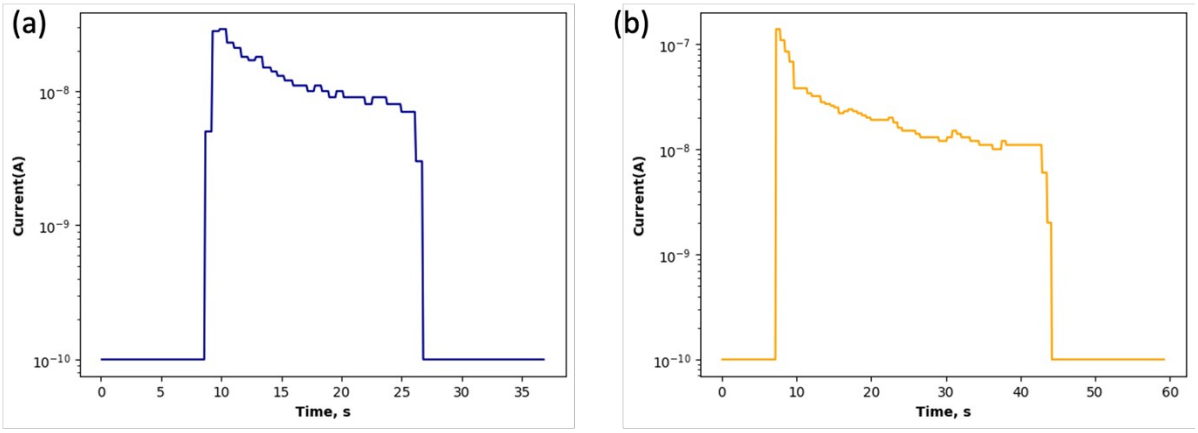

Figure S18. Retention time for both groups: (a) memristor exposed to a humid environment and (b) memristor placed in an inert nitrogen atmosphere.

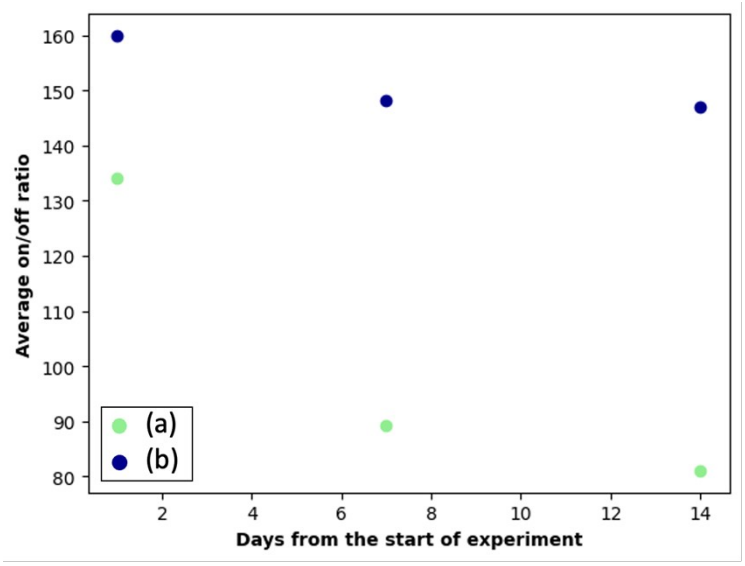

Figure S19. Dependence of the average ON/OFF ratio for memristive switching as a function of time from the start of the experiment for both groups: (a) memristor exposed to a humid environment and (b) memristor placed in an inert nitrogen atmosphere.

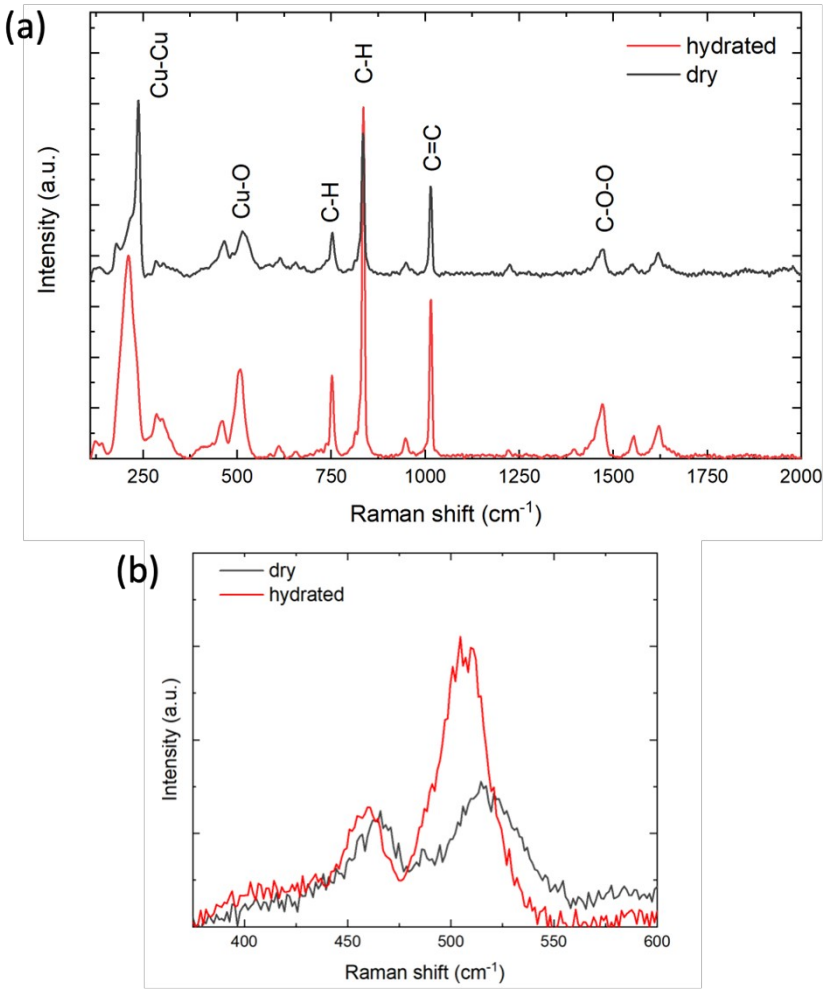

Figure S20. Raman spectroscopy of samples, presented on Figure S16.

11. References

1 G. Ding, J. Zhao, K. Zhou, Q. Zheng, S.-T. Han, X. Peng and Y. Zhou, *Chem. Soc. Rev.*, 2023, **52**, 7071–7136.

2 N. Kulachenkov, Q. Haar, S. Shipilovskikh, A. Yankin, J.-F. Pierson, A. Nominé and V. A. Milichko, *Adv. Funct. Mater.*, 2022, **32**, 2107949.

3 L. Zhao, W. Wu, X. Shen, Q. Liu, Y. He, K. Song, H. Li and Z. Chen, *ACS Appl. Mater. Interfaces*, 2019, **11**, 47073–47082.

4 Y. Liu, H. Wang, W. Shi, W. Zhang, J. Yu, B. K. Chandran, C. Cui, B. Zhu, Z. Liu, B. Li, C. Xu, Z. Xu, S. Li, W. Huang, F. Huo and X. Chen, *Angew. Chem. Int. Ed.*, 2016, **55**, 8884–8888.

5 M.-J. Park and J.-S. Lee, *RSC Adv.*, 2017, **7**, 21045–21049.

6 K. He, Y. Liu, M. Wang, G. Chen, Y. Jiang, J. Yu, C. Wan, D. Qi, M. Xiao, W. R. Leow, H. Yang, M. Antonietti and X. Chen, *Adv. Mater.*, 2020, **32**, 1905399.

7 X. Mao, M. Qian, X. Xuan, Y. Gao, Y. Niu and S. Gong, *Phys. Rev. Appl.*, 2022, **17**, 064004.

8 L. Pan, G. Liu, H. Li, S. Meng, L. Han, J. Shang, B. Chen, A. E. Platero-Prats, W. Lu, X. Zou and R.-W. Li, *J. Am. Chem. Soc.*, 2014, **136**, 17477–17483.

9 Z. Yao, L. Pan, L. Liu, J. Zhang, Q. Lin, Y. Ye, Z. Zhang, S. Xiang and B. Chen, *Sci. Adv.*, 2019, **5**, eaaw4515.

10 Y. J. Jeon, H. An, Y. Kim, Y. P. Jeon and T. W. Kim, *Appl. Surf. Sci.*, 2021, **567**, 150748.

11 S. M. Yoon, S. C. Warren and B. A. Grzybowski, *Angew. Chem. Int. Ed.*, 2014, **53**, 4437–4441.

12 T. Nhu Hoang Tran, T. Hoang Le, H. Kieu Thi Ta, Y. Thi Dang, L. Thuy Ho Nguyen, T. Hoang Le Doan, C.-K. Fang, I.-S. Hwang, T. Bach Phan and N. K. Pham, *Org. Electron.*, 2021, **93**, 106136.

13 N. Burshtein, S. T. Chan, K. Toda-Peters, A. Q. Shen and S. J. Haward, *Curr. Opin. Colloid Interface Sci.*, 2019, **43**, 1–14.

14 S. J. Haward, C. C. Hopkins and A. Q. Shen, *Proc. Natl. Acad. Sci.*, 2021, **118**, e2111651118.

15 C. W. Hirt and B. D. Nichols, *J. Comput. Phys.*, 1981, **39**, 201–225.

16 J. U. Brackbill, D. B. Kothe and C. Zemach, *J. Comput. Phys.*, 1992, **100**, 335–354.

17 N,N-Dimethylformamide (DMF) Dynamic Viscosity - SpringerMaterials, https://materials.springer.com/thermophysical/docs/vis_c72, (accessed May 5, 2024).

18 3M™ Fluorinert™ Electronic Liquid FC-40, https://www.3m.com/3M/en_US/p/d/b40045180/, (accessed May 5, 2024).

19 A. A. Yakovenko, J. H. Reibenspies, N. Bhuvanesh and H.-C. Zhou, *J. Appl. Crystallogr.*, 2013, **46**, 346–353.

20 N. K. Kulachenkov, D. Sun, Y. A. Mezenov, A. N. Yankin, S. Rzhevskiy, V. Dyachuk, A. Nominé, G. Medjahdi, E. A. Pidko and V. A. Milichko, *Angewandte Chemie International Edition*, 2020, **59**, 15522–15526.